Binding energy of charged excitons in ZnSe-based quantum wells

G. V. Astakhov and D. R. Yakovlev
Physikalisches Institut der Universität Würzburg, 97074 Würzburg, Germany
and A.F. Ioffe Physico-Technical Institute, Russian Academy of Sciences, 194017, St. Petersburg, Russia

V. P. Kochereshko
A.F. Ioffe Physico-Technical Institute, Russian Academy of Sciences, 194017, St. Petersburg, Russia

W. Ossau and W. Faschinger
Physikalisches Institut der Universität Würzburg, 97074 Würzburg, Germany

J. Puls and F. Henneberger
Humboldt-Universität zu Berlin, Institut für Physik, 10115 Berlin, Germany

S. A. Crooker and Q. McCulloch
National High Magnetic Field Laboratory, Los Alamos, New Mexico 87545

D. Wolverson
University of Bath, BA2 7AY Bath, United Kingdom

N. A. Gippius
General Physics Institute, Russian Academy of Sciences, 117333 Moscow, Russia

A. Waag
Abteilung Halbleiterphysik, Universität Ulm, 89081 Ulm, Germany
(Received 2 November 2001; published 12 April 2002)

Excitons and charged excitons (trions) are investigated in ZnSe-based quantum well structures with (Zn,Be,Mg)Se and (Zn,Mg)(S,Se) barriers by means of magneto-optical spectroscopy. Binding energies of negatively (X^-) and positively (X^+) charged excitons are measured as functions of quantum well width, and free carrier density and in external magnetic fields up to 47 T. The binding energy of X^- shows a strong increase from 1.4 to 8.9 meV with decreasing quantum well width from 190 to 29 Å. The binding energies of X^+ are about 25% smaller than the X^- binding energy in the same structures. The magnetic field behavior of X^- and X^+ binding energies differ qualitatively. With growing magnetic field strength, X^- increases its binding energy by 35–150%, while for X^+ it decreases by 25%. Zeeman spin splittings and oscillator strengths of excitons and trions are measured and discussed.

DOI: 10.1103/PhysRevB.65.165335 PACS number(s): 73.21.Fg, 71.10.Ca, 71.35.−y, 78.66.Hf

I. INTRODUCTION

Charged excitons (or trions) are exciton complexes consisting of three particles. Two electrons and one hole form a negatively charged exciton X^-. Two holes and one electron can be organized in a positively charged exciton X^+. Trion complexes in bulk semiconductors, i.e., in three dimensions, are fragile, but become stable in low-dimensional systems. That is why the theoretical prediction of Lampert from 1958[1] was followed by a confident experimental observation of trions only in 1993 for the quasi-two-dimensional electronic system in CdTe/(Cd,Zn)Te quantum wells (QW's).[2] Since then, positively and negatively charged excitons have been studied experimentally in III-V heterostructures based on GaAs and in II-VI quantum well structures based on CdTe, (Cd,Mn)Te, ZnSe, and (Zn,Mn)Se (see, e.g., Refs. 3–6 and references therein).

II-VI semiconductors are very suitable for the trion studies due to their strong Coulombic interaction compared with III-V materials, e.g., exciton binding energies (exciton Rydberg) in GaAs, CdTe, and ZnSe are 4.2, 10, and 20 meV, respectively. Among these materials ZnSe has the strongest Coulombic interaction. However, after the first report of an X^- observation in $Zn_{0.9}Cd_{0.1}Se$/ZnSe QW's in 1994,[7] detailed investigations started from 1998 only, when the high-quality ZnSe-based structures with binary quantum well layers were fabricated.[8–10] At present rather detailed experimental information on trions in ZnSe QW's is available: (i) negatively and positively charged excitons were documented;[5] (ii) trions were reported for the light-hole excitons;[5,8] (iii) singlet and triplet trion states were studied in high magnetic fields;[11,12] (iv) the spin structure of trions and spin-dependent formation process of trions were investigated;[11,13] (v) recombination dynamics in magnetic fields[14] and coherent dynamics of trions[15] were studied; and (vi) the oscillator strength of trion resonances was examined for different electron densities and in magnetic fields.[16] Theoretical results for this material system are limited to a cal-

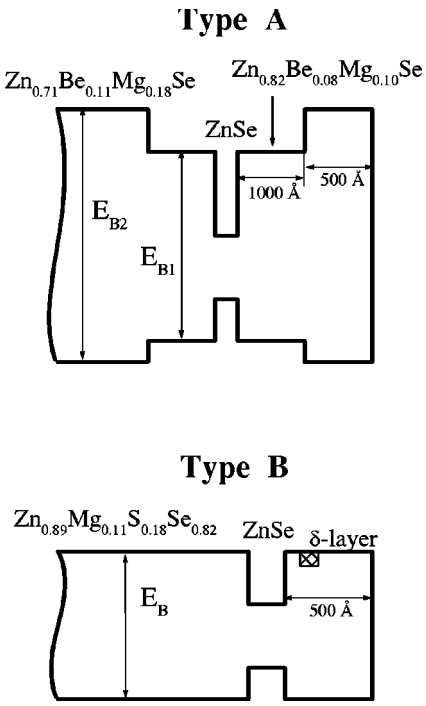

FIG. 1. Schematics of the studied structures. Type A is a $ZnSe/Zn_{0.82}Be_{0.08}Mg_{0.10}Se$ single QW surrounded by an additional $Zn_{0.71}Be_{0.11}Mg_{0.18}Se$ barrier. Type B is a ZnSe/$Zn_{0.89}Mg_{0.11}S_{0.18}Se_{0.82}$ single QW with modulation doping.

culation of the trion binding energy versus well width[17] and its variation in high magnetic fields.[12] Agreement with experiment was rather qualitative—one of the reasons for this is the uncertainty in the parameters used for the calculations.

In this paper we present a detailed study of trion binding energies in ZnSe-based structures as a function of quantum well width and applied magnetic field. Parameters of exciton and trion states were determined by means of magneto-optical experiments, calculated on the basis of the variational approach, and evaluated from the best fit of the experimental dependencies. The paper is organized as follows: Section II details the structures, while exciton parameters (measured and calculated) are discussed in Sec. III. In Sec. IV results on the binding energies of trions are collected and discussed. Finally, in Sec. V results of a modification of the singlet trion state in high magnetic fields and with increasing carrier density are presented.

In this paper we deal with positively (X^+) and negatively (X^-) charged excitons. We will label them in this way when the difference in the charge structure of trions is important. The term trion (T) will be used as a general definition for both positively and negatively charged excitons.

II. EXPERIMENT

Quantum well structures. ZnSe-based quantum well heterostructures with a binary material of QW were grown by molecular-beam epitaxy on (100)-oriented GaAs substrates. Studied structures contain single quantum wells, with thickness varying from 29 to 190 Å. Schemes for the structure designs are presented in Fig. 1. Different barrier materials were used, namely (Zn,Be,Mg)Se, (Zn,Mg)(S,Se), and (Zn,Be)Se, as shown in Table I. To each barrier material the type of a structure (A, B, C or D) has been assigned. Parameters of the barrier materials were chosen with an aim to make them lattice-matched to GaAs substrates, which allows growing QW's of a very high structural quality.

Most of the structures used in this study were nominally undoped (types A, C, and D). The background carrier density in them was tuned by an additional above-barrier illumination. The range of tuning depends on the QW width, which allows in the widest QW variation of electron density from 5×10^9 to 10^{11} cm^{-2}. Details of the illumination technique will be presented in Sec. IV B. Two structures of type B were modulation-doped in the barrier layers. In the sample zq1038 free electrons in the QW were provided by *n*-type doping with a 30-Å-thick, Cl-doped layer (donor concentration of 5×10^{17} cm^{-3}) separated from the QW by a 100-Å-thick spacer. The sample zq1113 was *p*-type doped with nitrogen (rf plasma cell at a power of 350 W and a background pressure of 5×10^{-6} Torr). In this sample, symmetric doping was achieved by uniform doping of barriers excluding 30-Å-thick spacer layers. The concentration of the two-dimensional hole gas (2DHG) in the QW of this sample is about $n_h\approx3\times10^{10}$ cm^{-2} and was insensitive to additional illumination.

Strain effect on the band gap. ZnSe quantum well layers in the studied structures experience compressive strain due to a small difference in lattice constants of ZnSe and GaAs.

TABLE I. Parameters of the barrier materials in ZnSe-based QW's with a type-I band alignment at $T=1.6$ K.

Material	Type	Barrier band gap, E_g^b(eV)	ΔE_g to ZnSe (meV)	$\Delta E_C/\Delta E_V$ to ZnSe
$Zn_{0.82}Be_{0.08}Mg_{0.10}Se$ "inner barriers" (B1)	A	3.06	240	78/22
$Zn_{0.71}Be_{0.11}Mg_{0.18}Se$ "outer barriers" (B2)	A	3.21	390	78/22
$Zn_{0.96}Be_{0.04}Se$	D	2.89	70	78/22
$Zn_{0.89}Mg_{0.11}S_{0.18}Se_{0.82}$	B	3.02	200	50/50
$Zn_{0.95}Mg_{0.05}S_{0.09}Se_{0.91}$	C	2.92	100	50/50

TABLE II. Parameters of ZnSe and ZnSe-based QW's with type-I band alignment.

"Unstrained" band gap E_g [a]	2.820 eV
Dielectric constant ε [a]	9.0
Elastic stiffness constants [b]	
C_{11}	8.26×10^{10} N/cm^{-2}
C_{12}	4.98×10^{10} N/cm^{-2}
Deformation potential [b]	
a	-4.25 eV
b	-1.2 eV
Elastic strain ϵ [c]	0.26%
Band gap corrections due to strain [d]	
Heavy-hole band ΔE_{hh}	2 meV
Light-hole band ΔE_{lh}	16 meV
Electron effective mass m_e [e]	$0.15m_0$
Heavy-hole effective mass along growth direction m_{hh}^z [f]	$0.8m_0$

[a]Reference 24.
[b]Reference 18.
[c]$\epsilon=[a_0(\mathrm{ZnSe})-a_0(\mathrm{GaAs})]/a_0(\mathrm{GaAs})$.
[d]Calculation according to Ref. 19.
[e]Reference 25.
[f]Because of uncertainty in heavy-hole effective mass given in the literature (values are in the range 0.6-1.0), for determination of the heavy-hole effective mass we take Luttinger parameters $\gamma_1=2.45$, $\gamma_2=0.61$, which were determined in Ref. 26 from two-photon magnetoabsorption measurements.

This results in an increase of the band gap, which is different for the heavy-hole and light-hole states (for details see, e.g., Refs. 18 and 19). The calculated values of the band gap increase give 2 meV for the heavy-hole states and 16 meV for the light-hole states (required parameters of the elastic stiffness constants C_{11}, C_{12} and deformation potentials a, b are given in Table II).

Band offsets. (Zn,Be,Mg)Se or (Zn,Mg)(S,Se) barrier materials differ by their band gap discontinuity to the ZnSe quantum well ΔE_g and its distribution between the conduction and valence bands $\Delta E_C/\Delta E_V$ (where $\Delta E_C+\Delta E_V=\Delta E_g$). The band gap discontinuity between the gap of ZnSe $E_g(\mathrm{ZnSe})=2.82$ eV (at $T=1.6$ K) and the barrier gap is distributed between conduction and valence bands in proportion $\Delta E_C/\Delta E_V=78/22$ for ZnSe/(Zn,Be,Mg)Se heterointerface.[20] For the ZnSe/(Zn,Mg)(S,Se) heterosystem, different values can be found in the literature varying from 50/50 (Refs. 21 and 22) to 10/90 (Ref. 23). We chose a 50/50 ratio for our calculation of the structure parameters. We believe that very similar values for trion binding energies measured in the both types of studied structures (to be shown in Fig. 16) justify a considerable confinement for electrons and, respectively, confirm our choice of $\Delta E_C/\Delta E_V$. In Sec. III we will use, for consideration of exciton parameters, published experimental data for ZnSe-based QW's with other barrier materials, namely, (Zn,Be)Se and (Zn,Mg)(S,Se) of lower content. Parameters for the barrier materials are collected in Table I.

Parameters of barrier alloys. Exciton energy of the barrier materials (E_X^b) has been evaluated directly from the exciton resonance in reflectivity spectrum measured at $T=1.6$ K. Taking for the exciton binding energy 20 meV (which is the value known for ZnSe) we estimate the band gap of the barrier E_g^b; this value is given in Table I. The band gap discontinuity to ZnSe (ΔE_g) is also included in the table. In the model calculations performed in Sec. III we will use values from Table I that are received from experiment.

To assign a certain composition of components in ternary and quaternary barrier materials the following considerations have been used. All structures were grown very closely lattice-matched to GaAs substrates, as confirmed by x-ray measurements. This condition gives us a ratio for the composition of different components in the quaternary alloys. For $Zn_{1-x}Mg_xS_ySe_{1-y}$ lattice-matched alloys the results of Refs. 27 and 28 have been used, which allow us to assign the barrier with $\Delta E_g=200$ meV to $Zn_{0.89}Mg_{0.11}S_{0.18}Se_{0.82}$ and the one with $\Delta E_g=100$ meV to $Zn_{0.95}Mg_{0.05}S_{0.09}Se_{0.91}$.

We give here more details for parameters we use for $Zn_{1-x-y}Be_xMg_ySe$ alloy parametrization, as literature data are rather limited and give large scattering. The band gap variation in ternary alloy $Zn_{1-y}Mg_ySe$ taken from Ref. 29,

$$E_g(\mathrm{Zn_{1-y}Mg_ySe})=E_g(\mathrm{ZnSe})+1.37y+0.47y(y-1), \quad (1)$$

agrees well with results given by different groups. For the band gap variation of $Zn_{1-x}Be_xSe$ alloys we utilize the results of Ref. 30, where the full range of contents from ZnSe to BeSe has been studied. The band gap of BeSe at room temperature was determined as 5.55 eV and the respective band gap variation for the alloy has been fitted by the following equation:

$$E_g(\mathrm{Zn_{1-x}Be_xSe})=E_g(\mathrm{ZnSe})+2.87x+1.1x(x-1). \quad (2)$$

For the relatively small values of cation substitution ($x,y<0.2$) it is reasonable to construct the band gap variation of the quaternary alloy $Zn_{1-x-y}Be_xMg_ySe$ as a linear combination of Eqs. (1) and (2):

$$E_g(\mathrm{Zn_{1-x-y}Be_xMg_ySe})=E_g(\mathrm{ZnSe})+2.87x+1.1x(x-1)+1.37y+0.47y(y-1). \quad (3)$$

Lattice matching of the quaternary alloy to the lattice constant of GaAs $a_0(\mathrm{GaAs})=5.653$ Å at $T=300$ K gives us a relationship for x and y ingredients of the alloy. Based on the lattice constants for the binary alloys [5.6676 Å for ZnSe, 5.1520 Å for BeSe, and 5.904 Å for MgSe (Ref. 24)] and the Vegard law,[31] the following dependencies for the lattice constants of ternary alloys (giving in Å) can be derived (for $T=300$ K):

$$a_0(\mathrm{Zn_{1-x}Be_xSe})=5.6676-0.516x, \quad (4)$$

$$a_0(\mathrm{Zn_{1-y}Mg_ySe})=5.6676+0.236y. \quad (5)$$

Lattice matching to GaAs corresponds to the ternary alloy $Zn_{0.971}Be_{0.029}Se$ and quaternary alloys satisfying a condition

$$y = 2.186x - 0.062. \tag{6}$$

Combining Eqs. (3) and (6), one can arrive at the following condition for the energy gap of the lattice-matched quaternary alloy:

$$E_g(\mathrm{Zn}_{1-x-y}\mathrm{Be}_x\mathrm{Mg}_y\mathrm{Se}) = E_g(\mathrm{ZnSe}) + 3.346x^2 + 3.61x - 0.054. \tag{7}$$

We derive the Be and Mg content in $Zn_{1-x-y}Be_xMg_ySe$ from experimental values of the enegy gap and with use of Eqs. (7) and (6). Respective data are given in Table I.

Experimental methods. Photoluminescence (PL), PL excitation, reflectivity (R), and spin-flip Raman scattering (SFRS) spectroscopies were exploited for experimental study of trion parameters. Optical spectra were detected at a low temperature $T=1.6$ K. Different cw lasers were used for photoexcitation, e.g., uv lines of an Ar-ion laser, a He-Cd laser, and a dye laser (Stylben 3). A halogen lamp was used in reflectivity experiments. External magnetic fields were applied along the structure growth axis (Faraday geometry). dc magnetic fields up to 7.5 T were generated by a superconducting solenoid and pulsed magnetic fields up to 47 T were used. In the case of dc field experiments direct optical access to the sample was available through windows. For pulsed field experiments fiber optics were used. In both cases circular polarization degree of emitted/reflected light was analyzed. A complete set of field-dependent PL spectra was collected during each magnetic field pulse (for details see Ref. 32). Experiments in a capacitor-driven 50-T midpulse magnet ($\sim$400-ms decay) were performed at the National High Magnetic Field Laboratory (Los Alamos, U.S.).

III. PROPERTIES OF CONFINED EXCITONS

In the studies of trions, similar to excitons, the Rydberg energy of the exciton in bulk semiconductor is often chosen as a characteristic energy to parametrize the problem. In the case of quantum confined heterostructures it is also instructive to compare the binding energies of trion states with the binding energies of confined excitons. We will follow this tradition in our investigations of charged excitons in ZnSe-based QW's. Published information on the properties of excitons (e.g., effective mass, binding energy, g factor, and radiative and nonradiative dampings, *etc.*) in ZnSe-based QW's with binary well material is rather limited. Therefore, we forestall the results on trions in this section where the exciton parameters for the ZnSe-based QW's will be evaluated from optical and magneto-optical experiments and from variational calculations.

A. Theoretical model for magnetoexcitons

In this section we will briefly describe the calculations of exciton levels in the quantum wells in the presence of a magnetic field directed along the growth axis. All the calculations of exciton states presented in this paper where made within a parabolic approximation, i.e., the admixture of the light-hole states and all effects of nonparabolicity are neglected. The quantization of the electron and hole states along the structure growth axis (z axis) provides us with the natural basis in the growth direction. We expand the wave function of the exciton in a series

$$\psi(\rho, z_e, z_h) = \sum A_{i,j,n}\xi_i(z_e)\zeta_j(z_h)\psi_n(\rho), \tag{8}$$

$\xi_i(z_e)$ and $\zeta_j(z_h)$ are the sets of solutions of the one-dimensional (1D) Schrödinger equation for electrons and holes in the z direction. The choice of the radial basis $\psi_n(\rho)$ will be discussed below.

Equation (8) represents the basis set for calculation of the exciton binding energy by diagonalization of the respective matrix. In the case of strong confinement (i.e., when the Coulomb interaction is significantly less than the separation between quantum confined states) one can neglect the excited single-particle states and the exciton problem reduces to a 1D radial equation with the Coulomb potential weighted over the ground states of the electron and hole [for $i,j=1$ in Eq. (8)].

However, in the case of shallow (or wide) QW's, where energy separation between levels of quantum confinement is small, such a reduction of the basis in the growth direction is not possible, and to calculate the spectrum of magnetoexcitons a numerical diagonalization scheme was used.[33] Although the solutions of the 1D radial equation are far from the real exciton wave functions they form an orthonormalized basis that can also be used in Eq. (8). Such choice of the radial expansion basis $\psi_n(\rho)$ allows evaluation of exciton parameters for a wide range of magnetic fields including the zero field limit, and provides better results for shallow QW's than the simple one-dimensional calculations. We present here the main line of this approach.

In the parabolic approximation, the QW electron-hole (e-h) Hamiltonian in the magnetic field $\mathbf{B}=(0,0,B)$ takes the form

$$H = H_{ez} + H_{hz} + H_{2\mathrm{D}} + U_{eh} \equiv H_0 + U_{eh}. \tag{9}$$

Here

$$H_{jz} = -\frac{\hbar^2}{2m_j^z}\frac{\partial^2}{\partial z_j^2} + V_j(z_j), \quad j = e,h. \tag{10}$$

$V_j = \Delta E_C$ (ΔE_V) is the band-offset potential in conduction (valence) band, and m_e^z and m_h^z are effective masses along the growth direction of the electron and the heavy hole, respectively. We will not account for weak anisotropy of electron effective mass in QW structures, i.e., take $m_e^z = m_e^{xy} = m_e$.

The Hamiltonian $H_{2\mathrm{D}}$ describes the two-dimensional (2D) motion of a free electron-hole pair in the magnetic field,

$$H_{2\mathrm{D}} = \frac{1}{2m_e}\left(-i\hbar\nabla\boldsymbol{\rho}_e + \frac{e}{c}\mathbf{A}_e\right)^2 + \frac{1}{2m_h^{xy}}\left(-i\hbar\nabla\boldsymbol{\rho}_h - \frac{e}{c}\mathbf{A}_h\right)^2, \tag{11}$$

where $\mathbf{A}_j = \frac{1}{2}\mathbf{B}\boldsymbol{\rho}_j$ is the vector potential in the symmetric gauge, $\boldsymbol{\rho}_{e(h)}$ are the in-plane coordinates of electron (hole),

TABLE III. Effective masses and parameters of Zeeman splitting for excitons and free carriers in ZnSe-based QW's. Values for effective masses are given in m_0. All experimental data, except g_e^{xy}, were measured in the Faraday configuration.

		Structure parameters			Effective mass		g factor						
		L_z	ΔE_g	Δ_{hh-lh}	μ	m_{hh}^{xy}	g_X		g_e^{xy}	g_e^z		g_{hh} [b]	
Sample	Type	(Å)	(meV)	(meV)			<10 T	40 T	SFRS	SFRS	Calc. [a]	<10 T	40 T
cb1175	A	29	240	24					1.21	1.17	1.13		
cb1173	A	48	240	20	0.119	0.58	1.0	1.3	1.17	1.17	1.13	2.2	2.5
cb1041	A	67	240	18	0.112	0.44	0.4	0.9			1.13	1.5	2.0
cb1174	A	67	240	17					1.13	1.13	1.13		
cb1198	A	95	240	13					1.11	1.11	1.12		
cb1172	A	190	240	11	0.107	0.37	0.4	0.4	1.11	1.11	1.12	1.5	1.5
zq1038	B	80	200	17					1.17	1.14	1.15		
zq1113	B	105	200	16	0.109	0.40	0.5	0.7			1.14	1.6	1.8
zq703	C	45	100	19	0.115	0.50	0.4	0.8			1.22	1.6	2.0

[a]From our calculation.

[b]Evaluated as $g_{hh}=g_e+g_X$, where g_e is corresponding g_e^z measured by SFRS or calculated in case if no experimental value is available.

$\rho=\rho_e-\rho_h=(x,y)$. We neglect here the mass difference in the well and barrier layers. The potential

$$U_{eh}(\rho,z_e,z_h)=-\frac{e^2}{\varepsilon}\left[\frac{1}{\sqrt{\rho^2+(z_e-z_h)^2}}\right] \tag{12}$$

is the Coulomb interaction between the electron and hole. ε is the dielectric constant.

The matrix elements of the Hamiltonian (9) in the basis (8) can be written in the following form

$$H_{i'j'n'}^{ijn}=(E_i^e+E_j^h+E_n^X)\delta_{ii'}\delta_{jj'}\delta_{nn'}+\langle ijn|U_{eh}|i'j'n'\rangle - \delta_{ii'}\delta_{jj'}\langle n|U_{11}^{11}|n'\rangle. \tag{13}$$

Here E_i^e and E_j^h are quantum confined energies of electrons and holes, E_n^X are the eigenvalues of the radial exciton equation with the Coulomb potential averaged over the ground electron and hole states $U_{11}^{11}(\rho)$. Here we have made use of the fact that basis functions $\psi_n(\rho)$ are the eigenfunctions of radial exciton Hamiltonian for the $\mathbf{K}=0$ s exciton (with the angular momentum projection of the relative e-h motion $l_z=0$) that reads as

$$H_\rho\psi_n(\rho)=E_n^X\psi_n(\rho),$$

$$H_\rho=-\frac{\hbar^2}{2\mu}\nabla_\rho^2+\frac{e^2B^2}{8\mu c^2}\rho^2+U_{11}^{11}(\rho), \tag{14}$$

where $\mu=(1/m_e+1/m_h^{xy})^{-1}$ is the reduced exciton mass, and

$$U_{ij}^{i'j'}(\rho)=\int dz_e\int dz_h U_{eh}(\rho,z_e,z_h)\xi_i(z_e) \times\xi_{i'}(z_e)\xi_j(z_h)\xi_{j'}(z_h), \tag{15}$$

$$\langle ijn|U_{eh}|i'j'n'\rangle=\int d^2\rho U_{ij}^{i'j'}(\rho)\psi_n(\rho)\psi_{n'}(\rho). \tag{16}$$

The diagonalization of Hamiltonian (13) provides us with both the eigenvalues and eigenfunctions of the exciton states. The dimension of the basis used depends on the relative values of the quantization energy and the Coulomb interaction. The wider the QW and, consequently, the smaller the vertical quantization, the larger the number of z functions taken into account. In our calculation we use all quantum confinement states in a real QW and ten radial basis functions. The parameters required for the calculations are the QW width (L_z), band offsets (ΔE_C, ΔE_V), effective masses of electron and hole in vertical direction (m_e, m_h^z), in-plane reduced exciton mass (μ), and dielectric constants (ε). We took ΔE_C, ΔE_V, m_e, m_h^z (namely m_{hh}^z for the heavy-hole exciton), and ε from the literature, and μ and L_z were obtained experimentally. The primary parameters are given in Tables I and II and the determined parameters are summarized in Tables III and IV.

In the frame of this approach we have calculated exciton energies for the studied QW structures versus QW width, exciton binding energies, and modification of these parameters in external magnetic fields up to 50 T. Results of these calculations are included in Figs. 4 and 5.

B. Optical spectra of excitons

Figure 2 displays typical optical spectra for three $ZnSe/Zn_{0.82}Be_{0.08}Mg_{0.10}Se$ single QW's, which cover the whole range of the studied QW widths L_z from 29 to 190 Å. Photoluminescence and reflectivity spectra were measured in the absence of external magnetic fields at a temperature of 1.6 K. Exciton resonances corresponding to the states formed with heavy and light holes (X_{hh} and X_{lh}, respectively) are clearly visible in reflectivity spectra. Trion resonances shifted to low energies from the X_{hh} energy are seen in 67- and 190 Å QW's. Their intensities in reflectivity spectra are proportional to the electron densities.[16] A low electron concentration and relatively large broadening make the trion resonance unresolvable for a 29-Å QW. For all structures shown, PL spectra consist of two lines, where the low-energy

TABLE IV. Energetic parameters of excitons and trions in ZnSe-based QW's at $T=1.6$ K.

		Exciton parameters							
						Binding			
		QW	Exciton	$E_{1s}-E_{2s}$		energy	Trion binding energy		
		width	energy, E_X	(meV)		(meV)	(meV)		
Sample	Type	(Å)	(eV)		Calc [a]	Calc [a]	X_{hh}^-	X_{lh}^-	X_{hh}^+
cb1175	A	29	2.8910		31.0	38.2	8.9		
cb1173	A	48	2.8472		27.5	34.0	6.6		
cb1048	A	64	2.8277	24.0	25.0	31.2	5.2		
cb1041	A	67	2.8260		24.7	30.7	5.3	4.0	
cb1174	A	67	2.8258		24.7	30.7	5.3		
cb1198	A	95	2.8149		21.7	27.3	4.0		
cb1172	A	190	2.8057		16.5	21.5	1.4		
zq1038	B	80	2.8182	25.0	22.7	28.5	4.4	3.6	3.3
zq1113	B	105	2.8129		20.6	26.1			3.1
zq703	C	50	2.8260	22.5	22.7	28.6			
cb571	D	50	2.8280		22.8	29.2	5.8	4.7	

[a]From our calculation.

line is due to the radiative recombination of negatively charged excitons (X_{hh}^-) and the high-energy line is due to recombination of neutral excitons (X_{hh}). Details of their identification in ZnSe-based QW's can be found in Ref. 5. With decreasing QW width, an increase of confined energies of carriers in the conduction and valence bands causes the high-energy shift of exciton transitions. It is accompanied by the broadening of exciton transitions due to QW width and barrier alloy fluctuations.

The full width at a half maximum (FWHM) of exciton and trion PL lines is plotted in Fig. 3. The exciton linewidth for $L_z>67$ Å is smaller than 1.2 meV, which gives evidence of the high structural and optical quality of the studied samples. For this range of QW width the trion linewidth roughly coincides with the exciton linewidth. It is interesting that for $L_z<100$ Å, exciton PL lines are narrower than the trion lines. The difference achieved 60% in a 29-Å QW. Possible reasons for this will be discussed in Sec. V D.

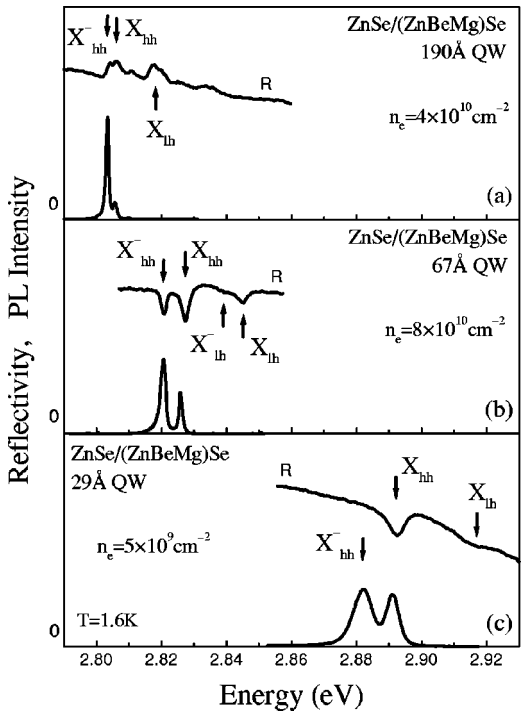

FIG. 2. Reflectivity and photoluminescence spectra taken from $ZnSe/Zn_{0.82}Be_{0.08}Mg_{0.10}Se$ (type A) structures with different QW widths of (a) 190 Å, (b) 67 Å, and (c) 29 Å. Arrows indicate the heavy-hole exciton (X_{hh}), the light-hole exciton (X_{lh}), and the negatively charged excitons (X_{hh}^- and X_{lh}^-). Electron concentration n_e in QW is given in the figure. $T=1.6$ K.

C. Excitons in high magnetic fields

Application of external magnetic fields allows the evaluation of important exciton parameters such as the in-plane reduced effective mass μ and the g factor that characterizes the spin splitting of excitons due to the Zeeman effect. These parameters are important for understanding and calculating

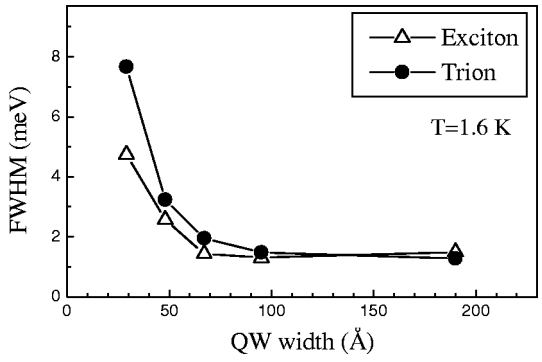

FIG. 3. Full width at a half maximum (FWHM) of trion (circles) and exciton (triangles) PL lines as a function of QW width in $ZnSe/Zn_{0.82}Be_{0.08}Mg_{0.10}Se$ structures. Lines are guides to the eye.

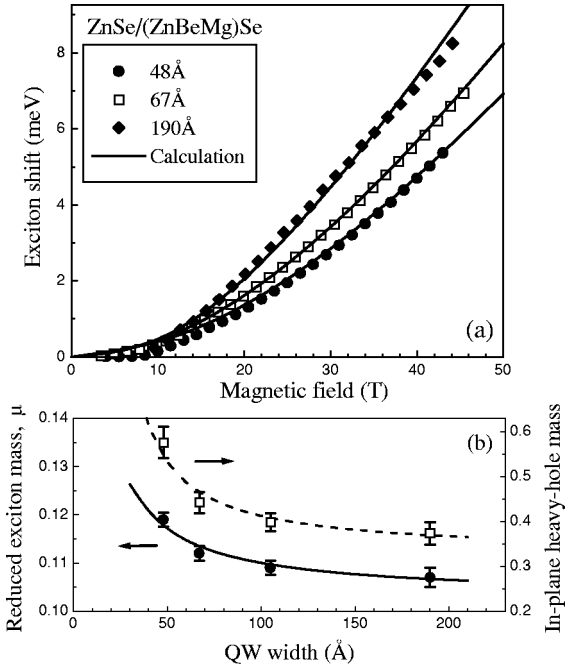

FIG. 4. (a) Exciton energy *vs* magnetic field strength for different type A QW's: 190 Å (diamonds), 67 Å (squares), and 48 Å (circles). The center of gravity of the exciton spin doublet in PL spectra is taken for the exciton energy. $T=1.6$ K. Lines show results of model calculations. (b) Reduced mass of exciton μ (left axis) and in-plane heavy-hole mass m_{hh}^{xy} (right axis) vs QW width. Symbols are experimental data. The solid line is an interpolation of data points by the hyperbolic function $\mu=(0.103+0.7/L_z[\text{Å}])m_0$. The dashed line is a result of calculation along $m_{hh}^{xy}=\mu m_e/(m_e-\mu)$.

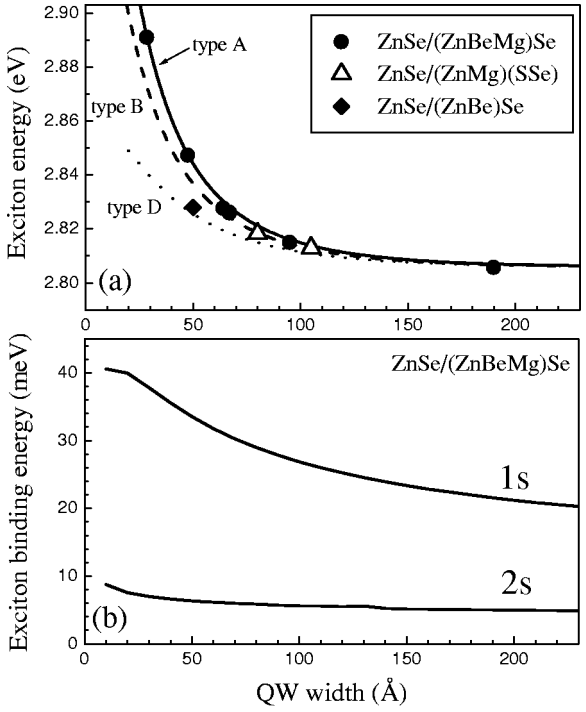

FIG. 5. (a) Lines are exciton energies calculated for different types of structures as a function of QW width. Symbols represent experimental data. The nominal (i.e., technological) values of QW width were slightly corrected to put experimental points at calculated dependencies. (b) The calculated exciton binding energy ($1s$ and $2s$ states) as a function of QW width for type A $ZnSe/Zn_{0.82}Be_{0.08}Mg_{0.10}Se$ structures.

the spin and energy structure of trions and excitons. Experiments were performed in pulsed magnetic fields to 47 T. Application of high magnetic fields was required to induce a sufficient energy shift of strongly bound excitons in ZnSe-based QW's. Photoluminescence spectra were measured in two circular polarizations corresponding to two spin states of optically active excitons. The evolution of PL spectra with increasing magnetic fields is discussed in detail in Refs. 8 and 12. Results on the spin splitting of excitons will be presented and discussed in Sec. III E. Here we concentrate on the energy shift of exciton with increasing magnetic fields.

To avoid spin splittings the center of gravity of the exciton spin doublet was evaluated and plotted as a function of magnetic field strength in Fig. 4(a) for QW's of different widths. A characteristic diamagnetic shift of excitons is seen for all samples. The exciton shift increases in wider QW's, which coincides with decreasing binding energy of excitons.

Solid lines in Fig. 4(a) show the best fit of experimental data in the frame of the model described in Sec. III A. Parameters used for the calculations were taken from Tables I and II. The exciton reduced mass μ is the only free parameter in the fit. Determined values of μ are included in Table III and also plotted in Fig. 4(b) versus L_z. The reduced mass increases for thinner QW's with functional dependence that can be interpolated as $\mu=(0.103+0.7/L_z[\text{Å}])m_0$ [see the solid line in Fig. 4(b)]. Taking the value of the electron effective mass $m_e=0.15m_0$ to be independent of the well width (this is valid as confinement energies in the studied structures are small and do not exceed 60 meV, and one should not expect a strong contribution of nonparabolicity in the conduction band to the electron effective mass), the in-plane values for the heavy-hole effective mass m_{hh}^{xy} are determined by means of the relationship $m_{hh}^{xy}=\mu m_e/(m_e-\mu)$. These values are displayed in Fig. 4(b) by open squares (right axis). One can see that m_{hh}^{xy} increases significantly from $0.37m_0$ in a 190-Å QW to $0.58m_0$ in a 48-Å QW. This fact should be accounted for in model calculations of trion binding energies versus QW width (e.g., Ref. 17).

D. Confined excitons

QW width dependencies for exciton energy E_X and exciton binding energy E_B^X were calculated by means of the model described in Sec. III A. Structure parameters used for the calculations are in Tables I, II, and III. Results of these calculations are displayed in Fig. 5.

In Fig. 5(a) calculated exciton energies for different types of structures (which differ by barrier heights and band offsets) are plotted by lines. We use these dependencies and experimental values of the exciton energies to determine QW width in the studied structures. Experimental data are shown by symbols and included in Table IV. Nominal values of the QW width evaluated from the technological parameters coincide with high accuracy to the calculated values.

In Fig. 5(b) binding energies of $1s$ and $2s$ exciton states are plotted as a function of L_z for $ZnSe/Zn_{0.82}Be_{0.08}Mg_{0.10}Se$ structures. One can see that in ZnSe QW's, the exciton binding energy E_B^X (i.e., the binding energy of the $1s$ state) has its maximum for QW's with $L_z \approx 20$ Å. This value is 40 meV, i.e., about twice as large as the bulk exciton Rydberg constant $R=20$ meV. This value indicates that in the ZnSe QW's, the exciton is quasi-two-dimensional, as its binding energy is considerably smaller than the binding energy in 2D limit, $4R=80$ meV.

E. Zeeman splitting of excitons and free carriers

The spin splitting of the exciton states is composed of the splitting of conduction and valence bands, which are characterized by the electron (g_e) and hole (g_{hh} or g_{lh} for the heavy-hole or light-hole subbands) gyromagnetic ratios (g values). Following Ref. 34 we define the exciton g factor as $g_X = g_{hh} - g_e$. Values of g factors depend on the band structure parameters. They can be calculated with high accuracy for the conduction band. Modeling of the g factors for the valence band is more complicated due to the mixing of heavy-hole and light-hole bands, whose splittings depend on the structure parameters (strain, quantum confinement, differences in band parameters of the barrier and QW materials) (see, e.g., Ref. 35). Detailed investigations of electron g factors in (Zn,Mg)Se and Zn(S,Se) alloys[36] and ZnSe/(Zn,Mg)(S,Se) QW structures[51] have been performed by means of spin-flip Raman scattering spectroscopy. It was shown that with a properly chosen set of band parameters, the five-band model calculations, which account for the off-diagonal spin-orbit coupling terms (TO model in Ref. 36), give a very good agreement for the band gap dependence of g_e in ZnSe-based ternary alloys. The g_e values for the quaternary alloy (Zn,Mg)(S,Se) are also in a reasonable agreement with model estimations.[36,37] Estimation for the barrier materials in our structures gives us $g_e = +1.32$ and $+1.38$ for $Zn_{0.95}Mg_{0.05}S_{0.09}Se_{0.91}$ and $Zn_{0.89}Mg_{0.11}S_{0.18}Se_{0.82}$, respectively. These values exceed the electron g factor in ZnSe $g_e = +1.12$ (see Ref. 36 and references therein).

A well width dependence of the electron g factor in $ZnSe/Zn_{0.89}Mg_{0.11}S_{0.20}Se_{0.80}$ QW's (which are practically identical to our samples with $Zn_{0.89}Mg_{0.11}S_{0.18}Se_{0.82}$ barriers and $\Delta E_g \approx 200$ meV) has been investigated in Ref. 37. Comparison with the model calculations allows the authors to conclude that in contrast to the alloys the three-band model is sufficient to calculate g factors in QW structures. Two additional factors should be accounted for in QW's. First, there is difference in the band parameters in the well and barrier materials. In ZnSe-base QW's with relatively low barriers with band gaps in the region of 2.8–3.1 eV, the main contribution comes from the difference in the spin-orbit splitting Δ_0. However, the change of Δ_0 is rather small in the case of the group II element to be substituted, but is large if the group VI element is altered. In other words, one can omit the variation of Δ_0 for the structures with (Zn,Be,Mg)Te barriers, but it should be accounted for in the case of (Zn,Mg)(S,Se) barriers. The second consideration specific to the QW structures is due to the anisotropy of the electron g factors. Its value is relatively small (usually less than 10% of g_e) and is controlled by the splitting of light-hole and heavy-hole states due to strain and confinement effects. Experimental values of g_e^z and g_e^{xy} obtained by spin-flip Raman scattering for the type A and B ZnSe QW's confirm the small value for g_e anisotropy (see Table III).

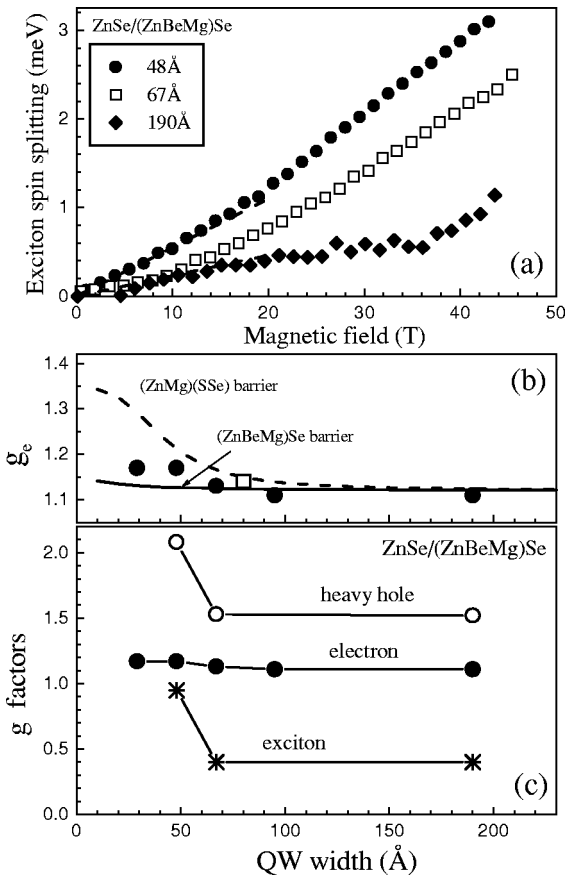

FIG. 6. (a) Zeeman splitting of exciton as a function of magnetic field for different QW widths: 190 Å (diamonds), 67 Å (squares), and 48 Å (circles). (b) Electron g factors g_e^z for QW's with type A (circles and solid line) and type B (squares and dashed line) barriers: lines are calculation and symbols are experimental data measured by spin-flip Raman scattering in the Faraday geometry. (c) g factors in $ZnSe/Zn_{0.82}Be_{0.08}Mg_{0.10}Se$ QW's. Exciton values for the low-field limit ($B<10$ T) are shown by stars. Solid circles present the electron g factor g_e^z. The heavy-hole g factor evaluated as $g_{hh} = g_e + g_X$ is given by open circles. Lines are guides to the eye.

The electron g factor for the type A QW's was measured by SFRS at the University of Bath. Details of experimental technique are published in Refs. 37 and 36. Experiments were performed in the Faraday and Voigt geometries to measure g_e^z and g_e^{xy} components of the electron g factor, respectively. Their values are included in Table III, and g_e^z are shown by solid circles in Figs. 6(b) and 6(c). Experimental data for an 80 Å $ZnSe/Zn_{0.89}Mg_{0.11}S_{0.18}Se_{0.82}$ QW were taken from Ref. 13 [shown by square in Fig. 6(b)].

Using the results of Ref. 37 we calculated average values for g_e in the structures of type A and type B. For the type A structures with (Zn,Be,Mg)Se barriers we use Eq. (7) from Ref. 37:

$$g_e(L_z)=g_e^{\mathrm{ZnSe}}+\frac{4\gamma E_P\Delta_0}{3E_X^3}. \quad (17)$$

Here ,$g_e^{\mathrm{ZnSe}}=+1.12$ is the electron g factor in ZnSe, $\gamma=E_X+E_B^X-E_g(\mathrm{ZnSe})$, $E_P=23.4$ eV is the squared momentum matrix element in ZnSe, $\Delta_0=0.42$ eV in ZnSe, E_X is exciton energy measured experimentally (see Table IV). The results are shown in Fig. 6(b) by a solid line. One can see that the g_e value is rather weakly dependent on the QW width for the whole studied range from 29 to 190 Å.

A more elaborate approach, accounting for the difference in Δ_0 for QW and barriers layers, was applied for the calculation of electron g factors in the type B QW's with (Zn,Mg)(S,Se) barriers. It is described by Eq. (8) from Ref. 37 and we do not detail it here. In this case g_e is more sensitive to the QW width for $L_z<100$ Å [see dashed line in Fig. 6(b)].

Hole g factors are strongly anisotropic (e.g., in-plane component of $g_{hh}\approx 0$), and their values are determined in a complicated manner on the splitting of heavy-hole and light-hole states $\Delta_{hh\text{-}lh}$ (see, e.g., Ref. 35). We are not aware of any simple calculation approach to this problem and will limit ourselves by experimental dependencies. Note that the bulk relation $g_{hh}=3g_{lh}$ is no longer valid in QW's.

Exciton Zeeman splittings in QW's of different thickness in Fig. 6(a) show reasonably good linear dependence on magnetic fields at $B<10$ T and some deviation from a linear behavior at high fields. It is well known that the nonlinearity of the exciton g factor is caused by the nonlinearity of its hole component g_{hh}, that in turn is due to the admixing of light-hole states in high magnetic fields. Electron Zeeman splittings, as a rule, shows a linear dependence over a wide range of magnetic fields, and this is true for ZnSe-based QW's.[37] To quantify the nonlinear spin splitting values we include in Table III two values for the exciton (g_X) and heavy-hole g factors estimated from linear interpolation of data points at low magnetic fields ($B<10$ T) and evaluated from the exciton spin splitting at $B=40$ T.

Exciton and carrier g factors for different QW's are collected in Table III and displayed in Fig. 6(c). In the figure the data are given for ZnSe/$Zn_{0.82}Be_{0.08}Mg_{0.10}Se$ QW's. Exciton values for the low-field limit ($B<10$ T) are shown by stars. In 190- and 67-Å QW's they are equal to $+0.4$ and g_X increases to $+1.0$ in a 48-Å QW. Solid circles trace the electron g factor g_e^z, which is weakly dependent on the well width. The heavy-hole g factor evaluated as $g_{hh}=g_e+g_X$ is given by open circles. Its dependence on the QW width reflects the g_X behavior.

Now we have all parameters necessary for analysis of the spin and energy structure of the trion states reported in this paper. Some further information on the exciton properties including radiative and nonradiative damping and coherent and recombination dynamics of excitons and trions in ZnSe-based QW's can be found in Refs. 14–16. We turn now to the main part of the paper, where the properties of charged excitons are investigated.

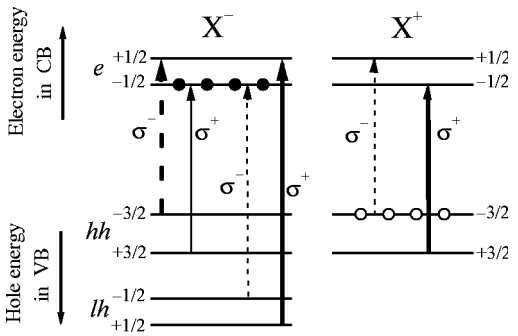

FIG. 7. Scheme of the optical transitions in ZnSe-based QW's for the creation of charged excitons in the cases of completely polarized 2DEG (solid circles) and 2DHG (open circles) induced by external magnetic fields. Optically active circular-polarized transitions are shown by arrows. The thick arrows represent the transitions in which the trion formation is allowed.

IV. CHARGED EXCITONS

A. Identification of negatively and positively charged excitons

Charged exciton states in optical spectra can be identified by their specific polarization properties in external magnetic fields. Analysis of the circular polarization degree of photoluminescence is rather complicated. In addition to the spin polarization of the free carriers, the spin-dependent trion formation and spin relaxation of trions are involved.[13] However, polarization properties of the trion states in reflectivity, absorption, or transmission spectra allow us to distinguish trions from excitons and positively and negatively charged excitons from each other. Here we present in short principles of the identification, and further details can be found in Refs. 5 and 16.

The polarization degree of the trion resonance in reflectivity spectra mirrors the polarization of free carriers in QW's, which is caused by thermal distribution of the carriers among the Zeeman sublevels. This is due to the singlet spin structure of the trion ground state, i.e., spins of two carriers with the same charges (electrons in X^- and holes in X^+) in the trion complex are oriented antiparallel. A triplet trion state with parallel orientation of these spins is unbound at zero magnetic field and becomes bound in high fields only.[12] When free carriers are fully polarized by magnetic field the trions can be excited optically only for one circular polarization. In case of negatively charged excitons in ZnSe QW's with a positive electron g factor it is σ^- polarization.

A scheme of the optical transitions responsible for trion excitation in strong magnetic fields is presented in Fig. 7. Spin-split states at the bottom of the conduction band and the top of the valence band are shown. Arrows indicate optical transitions where the absorbed light promotes an electron from the valence band to the conduction band and forms an exciton. Exciton generation in the presence of free carriers results in trion formation. Thick and thin arrows mark the allowed and forbidden transitions for the trion excitation in its ground state, when the carriers are fully polarized. It is clear from the scheme that X^- related to the heavy-hole and light-hole excitons will appear in opposite polarizations.

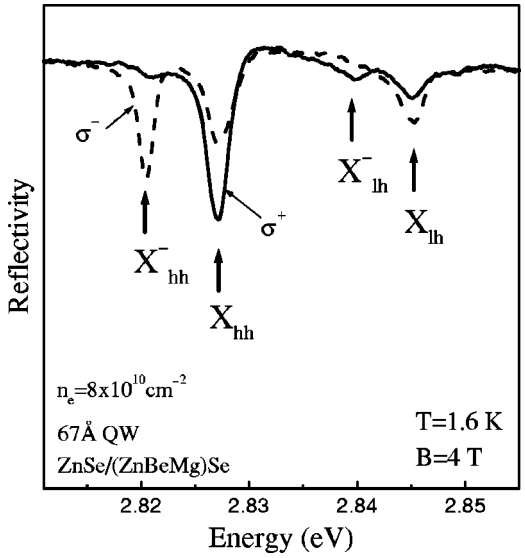

FIG. 8. Reflectivity spectra taken from a 67-Å $ZnSe/Zn_{0.82}Be_{0.08}Mg_{0.10}Se$ QW detected in different circular polarizations at a magnetic field of 4 T. Strongly polarized resonances of negatively charged excitons related to the heavy-hole (X^-_{hh}) and the light-hole (X^-_{lh}) excitons are labeled by arrows. The electron concentration in QW is $n_e=8\times10^{10}$ cm^{-2}, $T=1.6$ K.

Also X^- and X^+ in ZnSe QW's, where electron and hole g factors are positive, can be clearly distinguished by their opposite polarizations.

In Fig. 8 typical reflectivity spectra containing strongly polarized resonances of negatively charged excitons associated with heavy-hole excitons (X^-_{hh}) and light-hole excitons (X^-_{lh}) are given. Results are shown for a 67-Å $ZnSe/Zn_{0.82}Be_{0.08}Mg_{0.10}Se$ QW and a magnetic field of 4 T. In accordance with the selection rule discussed above, X^-_{hh} and X^-_{lh} resonances appear in different polarizations, i.e., σ^- and σ^+ respectively. Examples of the opposite polarization of X^- and X^+ in ZnSe QW's can be found in Ref. 5 and in Fig. 10 in the next section, where a recharging effect of the QW by above-barrier illumination is discussed.

B. Optical tuning of carrier density in QW's

Optical tuning of a carrier density in QW's is a very reliable method that is widely exploited for trion studies.[4,38–40] Different structure designs have been suggested for this purpose. The principle of the method is in the spatial separation of electron-hole pairs photogenerated by photons with energies exceeding the barrier band gap. Depending on the structure design, one type of carrier is captured by the surface states, trapped centers in barriers, or an additional quantum well. The other type of carrier is collected into the quantum well, where it is involved in trion formation. Free carrier concentration in the QW is tuned by the intensity of the above-barrier illumination. However, the dependence of the concentration on the illumination intensity can be very nonlinear with a pronounced saturation at higher intensities. The optical method can be also used for a fine tuning of carrier densities in structures with modulation doping and/or under applied gated voltage.

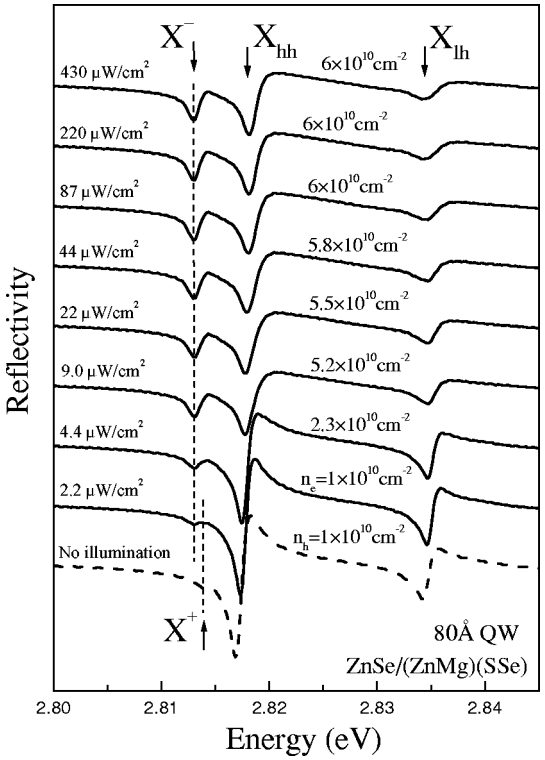

FIG. 9. Tuning of electron (hole) gas concentration by additional above-barrier illumination. The figure presents reflectivity spectra of an 80-Å $ZnSe/Zn_{0.89}Mg_{0.11}S_{0.18}Se_{0.82}$ QW *vs* illumination intensity of Ar-ion laser (3.5 eV). The laser power is given in the figure. $B=0$ T, $T=1.6$ K.

We will show here that optical tuning is very effective for the types A and B of ZnSe-based heterostructures investigated in this paper. Let us start with the type B structure zq1038, where the 80-Å QW is separated from the surface by a 600-Å $Zn_{0.89}Mg_{0.11}S_{0.18}Se_{0.82}$ barrier. Reflectivity spectra measured under different illumination intensities are presented in Fig. 9. Laser light with $\hbar\omega_L=3.5$ eV was used for illumination, and the high-energy part of the halogen lamp spectrum was cut by a 420-nm edge filter. Without laser illumination strong exciton resonances X_{hh} and X_{lh} dominate the reflectivity spectrum shown by a dashed line. Only a weak X^+ resonance is detectable 3.3 meV from the X_{hh} resonance to low energies. With increasing illumination power the X^+ resonance vanishes and a new X^- resonance appears. Its energy distance from the exciton energy is 4.4 meV. We note here that the same trick has been done in Ref. 4 for GaAs-based QW's. It is elegant and very convincing, as it allows measuring parameters of X^+ and X^- resonances in the same structure, thus avoiding technological and growth uncertainties.

Identification of charged exciton resonances were based on their polarization properties in external magnetic fields (see Fig. 10). We conclude from the data of Fig. 9 that without illumination all donor electrons from the modulation-doped layer are either captured by charged surface states or remain on donors. In this condition the QW contains a very diluted hole gas with $n_h=1\times10^{10}$ cm^{-2}. This value was determined from the oscillator strength of the X^+ transition,

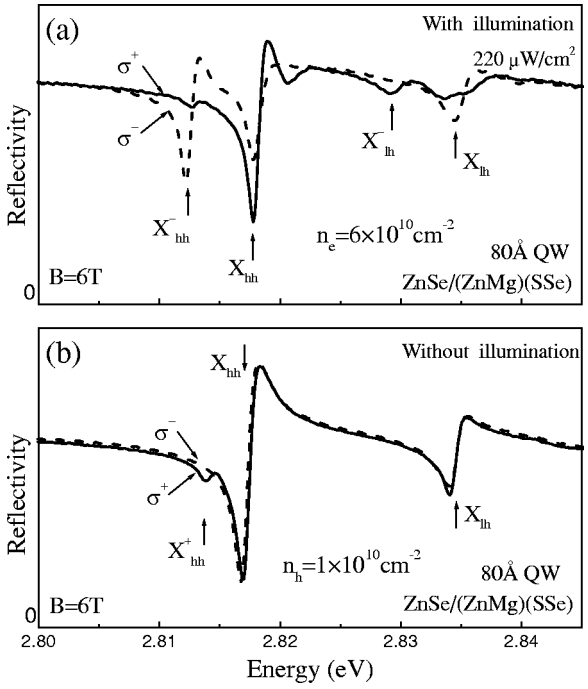

FIG. 10. Reflectivity spectra of an 80-Å $ZnSe/Zn_{0.89}Mg_{0.11}S_{0.18}Se_{0.82}$ QW: (a) With above-barrier illumination detected at different circular polarization at a magnetic field of 6 T. Arrows indicate negatively charged exciton (X^-) and excitons formed with heavy holes and light holes. (b) Without above-barrier illumination at a magnetic field of 6 T. Arrows indicate positively charged exciton (X^+) and excitons formed with heavy holes and light holes. $T=1.6$ K.

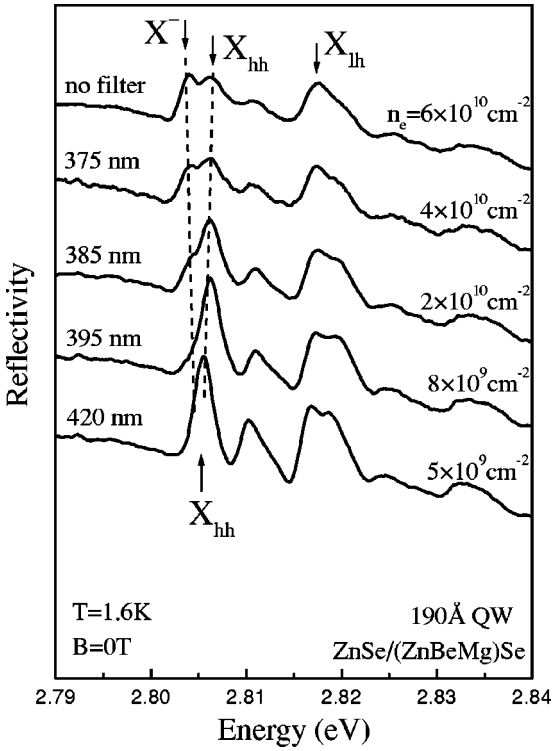

FIG. 12. Tuning of electron gas concentration by an additional above-barrier illumination. The figure presents reflectivity spectra taken from a 190-Å $ZnSe/Zn_{0.82}Be_{0.08}Mg_{0.10}Se$ QW as a function of above-barrier illumination. The illumination is provided by a white-light source together with long-pass optical filters having different absorption edges. The values of the filter absorption edge are given in the figure. $B=0$ T, $T=1.6$ K.

which for low carrier densities is linearly proportional to the carrier concentration (see details in Refs. 16 and 41). Laser illumination redistributes the carrier location in the structure by supplying the QW with electrons. An increase of the electron density saturates at $n_e=6\times10^{10}$ cm^{-2} (for detailed behavior see Fig. 11), which is still much lower than the concentration of donors in the modulation-doped layer $n_D=3\times10^{11}$ cm^{-2} evaluated from a technological calibration. We suggest that the reason is a relatively small conduction band offset in this structure ($\Delta E_C=100$ meV). Internal electric fields caused by carrier separation, when only part of the electrons are removed from the donors, can compensate for the energy difference between the electron level in the QW and the barrier donor energy.

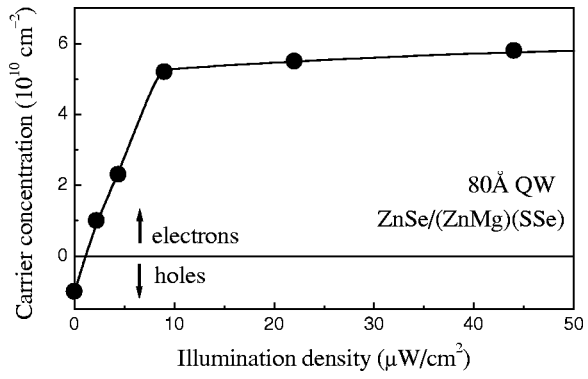

FIG. 11. Electron (hole) concentration in the QW as a function of illumination intensity. Symbols are experimental data (for details see Fig. 9); solid line is a guide to the eye. $T=1.6$ K.

In the type A structure cb1172, a 190-Å QW is separated from the surface by two barriers of different heights. Note that this structure is nominally undoped. Instead of the laser we use for illumination the light of the halogen lamp selected by edge filters. Reflectivity spectra are shown in Fig. 12. Only exciton transitions are visible in the spectrum measured with a 420-nm filter, i.e., when photocarriers are excited only in the ZnSe layer of the 190-Å-thick QW. A thresholdlike increase of the electron density in the QW starts when the energy of illumination light exceeds the band gap of the highest barrier (3.21 eV), as clearly seen in Fig. 13. The electron density in this structure is varied from 5×10^9 to 9×10^{10} cm^{-2}. n_e was evaluated from the analysis of the polarization degree of the trion line. The procedure has been suggested in Ref. 16 and detailed later in Ref. 41. It is based on the fitting of the magnetic-field-induced polarization of trion resonance in the frame of the approach accounting for the Fermi-Dirac statistics of the electron gas. Dashed lines in Fig. 14 show examples of the fitting. The Fermi energy that is determined from the best fit of experimental data points is directly linked to the electron density. From the thresholdlike effect of the illumination on the electron density in the QW

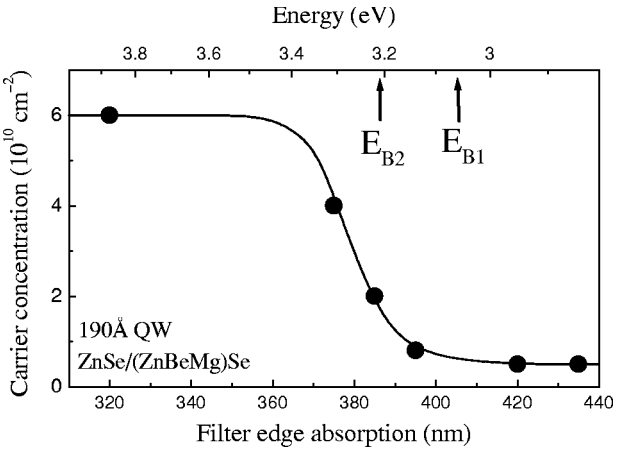

FIG. 13. Electron concentration as a function of wavelength of illuminating light. Symbols are experimental data from Fig. 12. Arrows show band gaps of barriers (see Fig. 1). Solid line is a guide to the eye.

shown in Fig. 14 we conclude that a recharging of surface states (namely a capture of photoholes by the surface states[42]) is the main mechanism for the carrier separation that supplies the QW with free electrons.

C. Exciton-trion energy separation: Effect of the Fermi energy

Now we turn our attention to the binding energy of the trions E_B^T, defined as the energy required to dissociate an isolated trion into a neutral exciton and an electron (for X^-) or a hole (for X^+). In the limit of a very diluted carrier gas, E_B^T is given by the energy difference between the exciton and trion lines (i.e., energy separation between bound and unbound states) $\Delta_{XT}=E_X-E_T$. A deviation from this "bare"

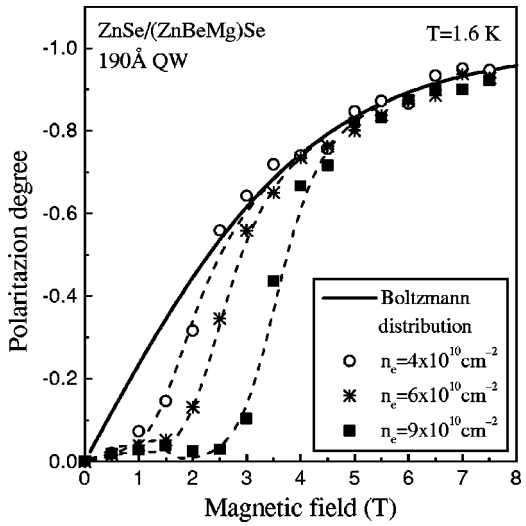

FIG. 14. Degree of circular polarization of a negatively charged exciton *vs* magnetic field for different 2DEG densities (n_e) in a 190-Å $ZnSe/Zn_{0.82}Be_{0.08}Mg_{0.10}Se$ QW. Symbols correspond to experimental data. The degree of circular polarization for the nondegenerate 2DEG with g factor $g_e=+1.12$ is shown by a solid line. Dashed lines represent fittings for the degenerate 2DEG; the obtained n_e are given in the figure. $T=1.6$ K.

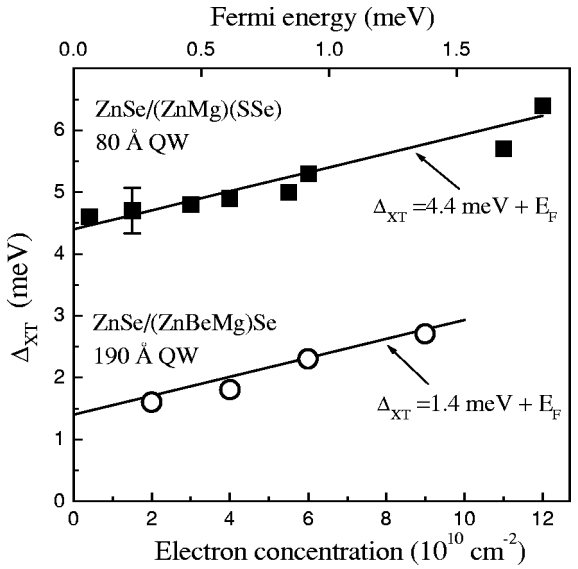

FIG. 15. Exciton-trion separation as a function of 2DEG density for a 190-Å $ZnSe/Zn_{0.82}Be_{0.08}Mg_{0.10}Se$ QW (circles) and an 80-Å $ZnSe/Zn_{0.89}Mg_{0.11}S_{0.18}Se_{0.82}$ QW (squares). Lines are the sum of a trion binding energy in corresponding QW and the Fermi energy of a 2DEG. $T=1.6$ K.

value of E_B^T takes place with increasing carrier density. It also has been shown in Ref. 43 that the trion linewidth and exciton-trion separation energy are modified by increasing temperature. The effect is due to the kinetic energy of the background electron before (after) the trion formation (recombination). At our experimental conditions at $T=1.6$ K, the electron kinetic energy is about 0.1 meV; with this reservation we will ignore in the following discussion the temperature contribution to Δ_{XT}.

In Fig. 15 we show the exciton-trion separation Δ_{XT} as a function of electron density n_e for two QW's. In the case of an 80-Å $ZnSe/Zn_{0.89}Mg_{0.11}S_{0.18}Se_{0.82}$ QW (squares) the electron concentration was varied by modulation doping. For a 190-Å $ZnSe/Zn_{0.82}Be_{0.08}Mg_{0.10}Se$ QW (circles) the electron density was tuned via additional illumination (see Sec. IV B). For both cases the exciton-trion energy separation increases remarkably with the electron density. Solid lines in Fig. 15 have a slope of the Fermi energy increasing with growing electron density $E_F=\pi\hbar^2 n_e/m_e$. In ZnSe QW's with $m_e=0.15m_0$ $E_F[\mathrm{meV}]=1.53\times10^{-11}n_e[\mathrm{cm}^{-2}]$. Comparing solid lines and data points in the figure one can establish that the concentration dependence of the exciton-trion energy separation is approximately given by the Fermi energy: $\Delta_{XT}=E_B^T+E_F$. This result has been also reported recently for CdTe-based QW's.[44]

Such a behavior of $\Delta_{XT}(n_e)$ does not correspond to a real increase of the trion binding energy and can be quantitatively explained in terms of exciton-trion repulsion due to their mixing.[45] This mixing is provided by mutual transformation of exciton and trion states via exchange of an additional electron. A detailed investigation of mixed exciton-trion states will be published elsewhere.

To obtain the E_B^T value we extrapolate experimental dependencies $\Delta_{XT}(n_e)$ to the limit $n_e\rightarrow0$ (see Fig. 15) getting

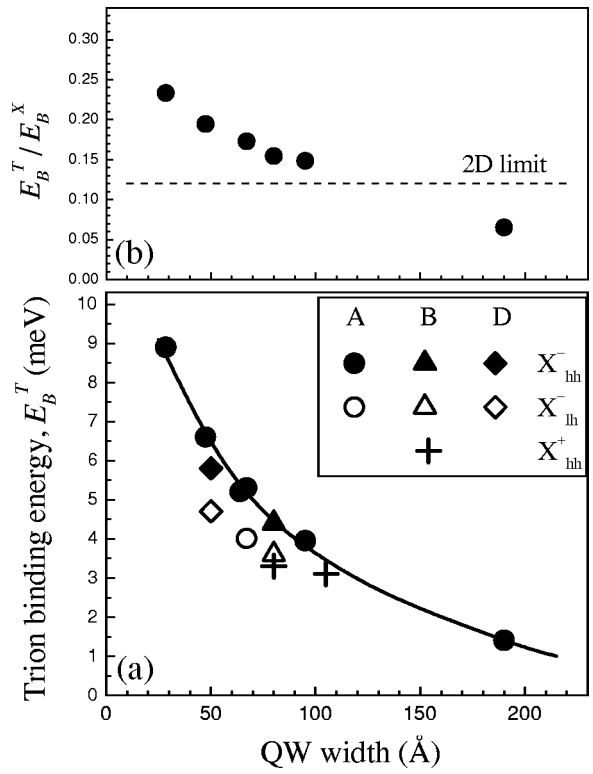

FIG. 16. (a) Trion binding energy as a function of QW width for $ZnSe/Zn_{0.82}Be_{0.08}Mg_{0.10}Se$ (type A), $ZnSe/Zn_{0.89}Mg_{0.11}S_{0.18}Se_{0.82}$, (type B) and $ZnSe/Zn_{0.96}Be_{0.04}Se$ (type D) structures. $T=1.6$ K. Solid symbols show data for negatively charged excitons formed with heavy holes (X^-_{hh}), open symbols are for negatively charged excitons formed with light holes (X^-_{lh}), and crosses are for positively charged excitons formed with heavy holes (X^+). The solid line is interpolation for X^-_{hh} values. The values of the trion binding energy are also given in Table IV. (b) Ratio of the X^-_{hh} binding energy to the binding energy of quasi-two-dimensional exciton taken from Fig. 5(b). The theoretical value of $E_B^T/E_B^X=0.12$ for a two-dimensional case is shown by a dashed line (Refs. 46 and 47).

the ''bare'' binding energy of trion E_B^T. We performed this procedure for all studied structures in order to receive information on binding energies of ''isolated'' trions that can be directly compared with theoretical calculations.

D. Binding energy of trions

Binding energies of trions E_B^T determined for the low carrier density regime are collected in Table IV and are displayed in Fig. 16(a) as a function of QW width. Solid symbols correspond to X^-_{hh}, open symbols show X^-_{lh}, and crosses are used for X^+_{hh}.

We discuss first the data for the negatively charged excitons related to heavy-hole excitons. The line in Fig. 16(a) is an interpolation made for X^-_{hh} data points (solid symbols). The trion binding energy increases strongly from 1.4 meV in a 190-Å QW up to 8.9 meV in a 29-Å QW. The increase for E_B^T is 6.4 times while the exciton binding energy increases only twice [see Fig. 5(b)]. The stronger sensitivity of the trion binding energy to confinement conditions is due to the larger extension of the trion wave function and to the strong effect of reduction of dimensionality on the trion stability.[48,49] Theoretical calculations show that trion states are very weakly bound in three-dimensional systems, which hinders their experimental observation in bulk semiconductors. Reduction of dimensionality from 3D to 2D is a crucial factor for increasing trion stability, and the trion binding energy grows by a factor of 10.[46] We believe that the increase of E_B^T shown in Fig. 16(a) is dominated by the localization of carrier wave functions along the structure growth axis, i.e., by the increasingly two-dimensional character of the carrier wave functions. Contribution of the in-plane localization of trions is minor except perhaps for the very narrow 29-Å QW. This conclusion is based on comparing the exciton linewidths (see Fig. 3), which gives us characteristic energies for the in-plane exciton localization, with the trion binding energies. The exciton linewidth is weakly sensitive to the QW width and is below 2 meV for the range 50–190 Å. It increases to 5.3 meV in the very narrow QW, but even in this case it stays smaller than the trion binding energy of 8.9 meV.

A detailed comparison of the trion and exciton modifications with decreasing QW width is given in Fig. 16(b), where the ratio of the trion and the exciton binding energies E_B^T/E_B^X is presented. For the 190-Å QW this ratio $E_B^T/E_B^X=0.065$. It increases linearly with decreasing QW width, achieving a value of 0.235 in the 29-Å QW. Theoretical calculations of this ratio performed for the two-dimensional limit give a value $E_B^T/E_B^X\approx 0.12$, which is rather insensitive to the ratio of electron and hole effective masses.[46,47] The experimental value for the 29-Å QW exceeds the theoretical limit by a factor of 2. We explain this by the fact that our experimental situation corresponds to the quasi-2D case rather than to strictly 2D one. This is confirmed by the moderate increase of the exciton binding energy, which is twice as large as the bulk Rydberg energy in narrow QW's and, respectively, twice as small as the 2D limit of four Rydberg constants. A dimensional transition for a Coulombic state in QW structures is determined by a ratio of the Bohr radius of the states to the QW width. Obviously, for trions with larger Bohr radius this transition will occur in wider QW's than for excitons, whose wave function is more compact. Thus at a given QW width, excitons and trions have different degrees of two-dimensionality, which causes a larger measured value of E_B^T/E_B^X compared with the calculated value for the 2D limit.

It is interesting to note that the strength of confinement potentials in our structures plays a minor effect on the trion binding energies. Data points in Fig. 16(a) for structures with different materials with ΔE_g value varied from 200 to 250 meV follow the same dependence. Only a small deviation from this dependence was found for the type D structure with $\Delta E_g=70$ meV. For very shallow 70 Å ZnSe/Zn(S,Se) QW's with $\Delta E_g=25$–35 meV a trion binding energy of 2.7–2.9 meV has been reported.[11] This is consistent with our data from Fig. 16(a) and evidences that decreasing the electron confinement leads to smaller binding energies for X^-.

We are aware of only one paper where the binding energies of X^-_{hh} were calculated for ZnSe-based QW's.[17] The

quantitative agreement was not satisfactory and the authors suggested that the polaron effect, which in ZnSe QW's could give an additional 1.3–2.6 meV contribution to the trion binding energy, should be considered. For our structures we found a relatively strong dependence of the exciton reduced mass on the QW width [see Fig. 4(b)]. We believe that incorporating this factor into calculations will increase their reliability and coincidence with experiment. Esser has run calculation for a 80-Å QW (zq1038) with our new parameters and obtained a value of 4.2 meV for X^-_{hh}, which is in good concordance with our experimental value of 4.4 meV even without the introduction of the polaronic correction.[50]

Binding energies of trions based on the light-hole excitons [open symbols in Fig. 16(a)] are 20–30% smaller than the X^-_{hh} binding energies. To the best of our knowledge no detailed investigation of X^-_{lh} states has been reported so far. Trions associated with light-hole excitons were observed in PL excitation spectra of GaAs-based QW's[51] and in the reflectivity spectra of monomolecular CdTe islands.[52] In both cases the X^-_{lh} binding energy was very close to that of X^-_{hh}. Numerical calculations performed for GaAs QW's give, for example, a 40% difference in favor of X^-_{hh} in a 100-Å $GaAs/Ga_{0.85}Al_{0.15}As$ QW.[48] However, the model used in Ref. 48 has not accounted for the modification of the in-plane effective mass in the valence band, which is essential for the quantitative comparison with experimental results.

It is interesting that positively charged excitons show binding energies reduced by about 25% compared with their negatively charged partners, e.g., in an 80-Å QW of type B (zq1038), binding energies for negatively and positively charged excitons are 4.4 and 3.3 meV, respectively. We are very confident of this result, as it has been measured in the same structure (see Figs. 9 and 10) where the type of the free carriers occupying the QW was reversed by the illumination. Calculations performed for the 3D and 2D limits give an X^+ binding energy larger than the X^- one;[46,47] this result is explained qualitatively by the heavier effective mass of holes compared to electrons. However, in the quasi-two-dimensional case the situation can differ qualitatively. Recent calculations performed by Esser with parameters of the structure zq1038 give 4.2 and 4.0 meV binding energies for X^- and X^+, respectively.[50] The smaller binding energy of the positively charged exciton is explained by the ''effective'' hole-hole Coulomb repulsion to be stronger in this QW than the electron-electron one. The calculations qualitatively reproduce experimental trends. Better quantitative agreement for the X^+ state is still desired. It is interesting to note that the calculations performed in Ref. 43 for a 250-Å-thick GaAs QW give a reversed order of binding energies for X^- and X^+ (0.8 and 1.0 meV, respectively). Possibly this is caused by weaker Coulomb interactions in III-V materials compared with II-VI materials. Experimentally similar values for binding energies of X^- and X^+ of 1 meV are found in a 200-Å-thick GaAs QW.[4]

Comprehensive theoretical consideration for the trion binding energy data collected in Fig. 16(a) is still missing. We hope that these data and the set of exciton parameters given in the paper will encourage such activity.

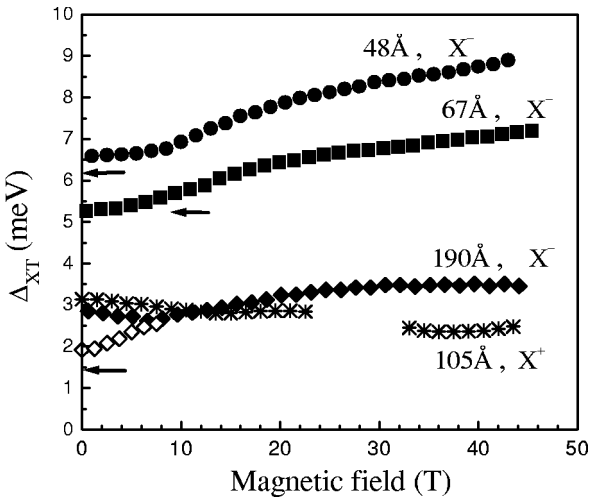

FIG. 17. Exciton-trion separation as a function of magnetic field for QW's of different width. X^- was measured in $ZnSe/Zn_{0.82}Be_{0.08}Mg_{0.10}Se$ QW's: 190 Å (diamonds), 67 Å (squares), 48 Å (circles). Solid symbols correspond to the PL excited by laser with energy above barrier and open symbols are for below-barrier excitation. Arrows indicate ''bare'' trion binding energy. X^+ is taken for a 105-Å $ZnSe/Zn_{0.89}Mg_{0.11}S_{0.18}Se_{0.82}$ QW's (stars). $T=1.6$ K.

V. PROPERTIES OF SINGLET TRION STATES

The singlet state is the ground state of a trion except at very high magnetic fields where the triplet state gains larger binding energy. Recently triplet states have attracted considerable attention in GaAs-based QW's[53,54] and in ZnSe-based structures.[12] However, this topic is outside the scope of the present paper and we concentrate here on the properties of the singlet state.

A. Magnetic field dependence of binding energy

The energy distance between exciton and trion PL lines Δ_{XT} is plotted in Fig. 17 versus magnetic field strength. In order to avoid uncertainties caused by spin splittings, data for the center of gravity of exciton and trion spin doublets are given. Our task is to study the binding energy of the ''bare'' trions that exhibit no contribution from the Fermi energy. The regime of the very diluted carrier gas is fulfilled for a 105-Å QW with X^+, where Δ_{XT} at $B=0$ T equals E_B^T (see Table IV). Similar statements can be made for 48- and 67-Å QW's with X^-. E_B^T values for QW's with X^- are shown by arrows. Only in the case of the 190-Å QW was the contribution of the Fermi energy to Δ_{XT} considerable for the set of data measured in pulsed magnetic fields (shown by solid diamonds in Fig. 17). We have repeated measurements for this structure in dc magnetic fields $B<8$ T, keeping the low density of a 2D electron gas (2DEG). Results are given by open diamonds. One can see that the difference between the two data sets vanishes with increasing magnetic fields and disappears for $B>7$ T. That means that the contribution of E_F decreases with growing magnetic fields, which can be explained by an increase of the density of states of the Landau levels. For the following discussion we consider the

$E_B^T(B)$ dependence for a 190-Å QW consisting of open diamonds at low fields and of solid diamonds at high fields ($B>8$ T).

Binding energies of X^- in all studied QW's show a monotonic increase with growing magnetic fields and a tendency to saturation in high fields $B>25$ T. The increase is stronger in wider QW's with smaller E_B^T, e.g., it amounts to 150% in a 190-Å QW and has only 35% in a 48-Å QW. Being more compact in narrow QW's the singlet state becomes less sensitive to compression by external magnetic fields. Qualitatively $E_B^T(B)$ dependencies for X^- from Fig. 17 are consistent with theoretical predictions for the singlet state.[12,53,55]

The magnetic field dependence of the positively charged exciton differs drastically from X^- behavior. Binding energy of X^+ shows no dependence on magnetic fields for $B<6$ T and decreases by 25% at higher fields (see stars in Fig. 17). In the field range 26–32 T the X^+ singlet state line shows irregular behavior caused by its crossing with the triplet state. These results will be published elsewhere and here, for clarity, we do not show data points for this field range. Principally different behavior of X^- and X^+ states in external magnetic fields has been established first for GaAs QW's.[4] Our results confirm this for ZnSe-based QW's. We are not aware of theoretical attempts to model X^+ behavior in magnetic fields. However, it is clear that the difference in magnetic field behavior of X^+ and X^- binding energies is due to the very different structure of wave functions of these complexes (see discussion in Ref. 47). X^- is constructed of two light particles (electrons) rotated around one heavy particle (hole). This complex has one center and magnetic field will localize the electron wave functions around the hole, thus inducing an increase of the binding energy. In contrast X^+ has two heavy particles, i.e. two centers, and one light particle moving between two centers. In this case the shrinking of the electron wave function by magnetic fields hinders it from optimal adjustment for two centers, which results in the decreasing binding energy of the X^+ complex.

B. Spin splitting of trions

In the studied structures, the Zeeman splitting of the trion singlet state closely follows the behavior of the exciton Zeeman splitting. Typical examples for 48- and 190-Å $ZnSe/Zn_{0.82}Be_{0.08}Mg_{0.10}Se$ QW's are given in Fig. 18. Deviations between exciton and trion splittings are inside the error bar of spectral resolution of 0.1 meV. This result is explained on the basis of a spin structure of trion and exciton states, suggesting that the electron and hole wave functions in a trion are the same as these in a neutral exciton (see, e.g., Refs. 12 and 53). Indeed the ground state of the negatively charged exciton exhibits a hole spin splitting as the two electrons with antiparallel spin orientation are insensitive to external magnetic fields. However, the Zeeman splitting of the trion optical transition must also reflect the Zeeman contribution of the bare electron, which remains after trion recombination. As a result, the Zeeman splitting of X^- is given by $g_{hh}-g_e$, which is identical to the exciton spin splitting. A similar consideration holds for the positively charged exciton.

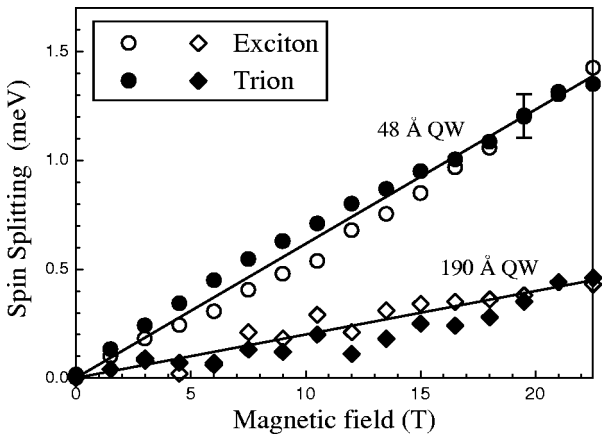

FIG. 18. Comparison of exciton and trion Zeeman splittings in $ZnSe/Zn_{0.82}Be_{0.08}Mg_{0.10}Se$ QW's. Symbols are experimental points; full curves are guidelines for the eye.

Different spin splitting of excitons and trions has been reported for a 200-Å GaAs-based QW and related to a different mixing of wave functions in X^- than in X.[4] Also for ZnSe/Zn(S,Se) QW's with a small confinement potential $\Delta E_g=35$ meV, different spin splittings of exciton and negatively changed exciton have been found.[11] We suppose that the small energy splitting between the heavy-hole and light-hole states in these structures allows mixing of these states in a trion that results in a modification of the hole g factor. In our structures Δ_{lh-hh} was relatively large, 11–20 meV (see Table III), which prevents the modification of the hole g factor.

C. Oscillator strength of trions

Treatment of resonances in reflectivity spectra allows extraction of the oscillator strength (i.e., radiative damping Γ_0) of trions and excitons. A detailed study of the trion oscillator strength in an 80-Å $ZnSe/Zn_{0.89}Mg_{0.11}S_{0.18}Se_{0.82}$ QW can be found in Ref. 16. It has been established experimentally that Γ_0^T increases linearly with electron concentration $\Gamma_0^T=Cn_e\Gamma_0^X$. The value of C is a very useful parameter for evaluation of the electron density by the optical method.[41]

In Fig. 19 Γ_0^T/Γ_0^X is plotted as a function of n_e for QW's of different thickness. The electron concentration was evaluated from the polarization properties of X^- in external magnetic fields (see, e.g., Fig. 14). The value of the slope C increases for wider QW's with smaller binding energies of trions. This is illustrated in the inset of Fig. 19 where C is plotted as a function of E_B^T. Trions with the smallest binding energy have the largest extension of wave function, which covers the largest number of unit cells and, respectively, gives the largest Γ_0^T value. Results from the inset of Fig. 19 confirm this conclusion. It is worthwhile to note that that these results also allow determination of a carrier density in ZnSe-based QW's of various widths.

D. Trion linewidth

We discuss here the linewidth of exciton and trion luminescence lines presented in Fig. 3. It was found that for

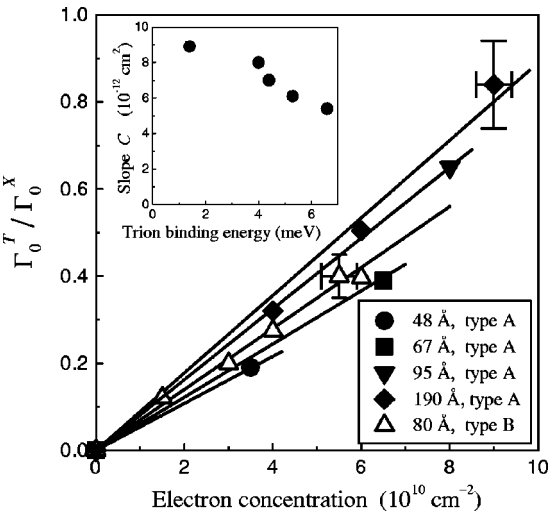

FIG. 19. Trion oscillator strength Γ_0^T normalized on the exciton one Γ_0^X vs electron density in different QW's. Lines show linear interpolation of experimental results. Slope of the dependence $\Gamma_0^T = Cn_e\Gamma_0^X$ as a function of trion binding energy is given by the inset. $T=1.6$ K.

QW's thinner than 100 Å, the trion line is systematically broader than the exciton line. The difference in linewidths increases up to 60% in a 29-Å QW. At least two physical reasons for that can be suggested: (i) The PL linewidth is contributed by localization energies for carriers. In the case of excitons it is summed up from the electron and hole contributions, where the electron plays a dominant role. In the case of trions, two electrons and one hole participate. Qualitatively it should result in larger broadening, but the quantitative approach to this problem does not seems to be very trivial, because it will depend strongly on the choice of a model for localizing potential. (ii) Another reason is related to a certain freedom in the energy conservation law in case of trion recombination. An electron, which is left after trion recombination, can have a finite kinetic energy. The energy of the emitted photon will be reduced by this amount. Respectively, the trion line will exhibit additional broadening due to the electron kinetic energy.

The first mechanism has a strong dependence on the QW width—its contribution should increase proportionally with growing broadening of the exciton line. However, the character of the well width dependence for the second mechanism is not very obvious for us.

The second mechanism has been studied theoretically and experimentally for GaAs-based QW's.[43] It was shown that it has a strong temperature dependence and at $T=2$ K the additional broadening of the trion line is about 0.04 of the exciton binding energy. Applying this estimation to our QW's we get the contribution of the second mechanism of 0.8 meV for a 190-Å QW and of 1.5 meV for a 29-Å QW. In the narrow QW, exciton and trion linewidths are 4 and 6.5 meV, respectively, i.e., they differ by 2.5 meV. From this we suggest that both mechanisms have a comparable contribution to the broadening of the trion emission line. Further experiments including the careful analysis of the temperature dependencies of the trion linewidth are required to separate the role of two mechanisms.

VI. CONCLUSIONS

Negatively and positively charged excitons in ZnSe-based QW's were investigated in structures with various QW widths and free carrier densities. The binding energy of X^- shows a strong dependence on the QW width, increasing from 1.4 to 8.9 meV as the well width decreases from 190 to 29 Å. This variation is 6.4 times while the neutral exciton binding energy increases only twice. The binding energy of X^+ is 25% smaller than that of X^-. This observation is in qualitative agreement with model calculations and is explained by stronger ''effective'' Coulomb repulsion in case of hole-hole interaction compared with electron-electron interaction. Qualitatively different behavior for X^- and X^+ is found in external magnetic fields. X^- increases its binding energy depending on the QW width by 35–150%, while in contrast X^+ shows a decrease of its binding energy by 25%. A detailed set of exciton parameters for the studied structures is collected in the paper. We hope that this will encourage theoretical efforts for a better understanding the energy and spin structure of trions.

ACKNOWLEDGMENTS

We acknowledge stimulating discussions with A. B. Dzyubenko and R. A. Suris. We are thankful to A. Esser for allowing us to use in this paper his unpublished results on the calculation of trion binding energies. The work was supported in part by the Deutsche Forschungsgemeinschaft through Sonderforschungbereich 410 and Grants No. Os98/6, No. 436 RUS 113/557, and No. He-1939/16-1, as well as by grants of the Russian Foundation for Basic Research (Grants No. 00-02-04020 and No. 01-02-04010).

[1] M.A. Lampert, Phys. Rev. Lett. **1**, 450 (1958).
[2] K. Kheng, R.T. Cox, Y.M. d'Aubigne, F. Bassani, K. Saminadayar, and S. Tatarenko, Phys. Rev. Lett. **71**, 1752 (1993).
[3] R.T. Cox, V. Huard, K. Kheng, S. Lovisa, R.B. Miller, K. Saminadayar, A. Arnoult, J. Cibert, S. Tatarenko, and M. Potemski, Acta Phys. Pol. A **94**, 99 (1998).
[4] S. Glasberg, G. Finkelstein, H. Shtrikman, and I. Bar-Joseph, Phys. Rev. B **59**, R10425 (1999).
[5] G.V. Astakhov, D.R. Yakovlev, V.P. Kochereshko, W. Ossau, J. Nürnberger, F. Faschinger, and G. Landwehr, Phys. Rev. B **60**, R8485 (1999).
[6] S.A. Crooker, E. Johnston-Halperin, D.D. Awschalom, R. Knobel, and N. Sarth, Phys. Rev. B **61**, R16307 (2000).
[7] K. Kheng, R.T. Cox, V.P. Kochereshko, K. Saminadayar, S. Ta-

tarenko, F. Bassani, and A. Franciosi, Superlattices Microstruct. **15**, 253 (1994).
[8] W. Ossau, D.R. Yakovlev, U. Zehnder, G.V. Astakhov, A.V. Platonov, V.P. Kochereshko, J. Nürnberger, F. Faschinger, M. Keim, and A. Waag, Physica B **256-258**, 323 (1998).
[9] S. Lovisa, R.T. Cox, T. Baron, M. Keim, A. Waag, and G. Landwehr, Appl. Phys. Lett. **73**, 656 (1998).
[10] V. Y. Ivanov, M. Godlewski, J.P. Bergman, B. Monemar, M. Behringer, and D. Hommel, in *Proceedings of the 24th International Conference on the Physics of Semiconductors, Jerusalem, Israel*, 1998 edited by D. Gershoni (World Scientific, Singapore, 1999).
[11] O. Homburg, K. Sebald, P. Michler, J. Gutowski, H. Wenisch, and D. Hommel, Phys. Rev. B **62**, 7413 (2000).
[12] D.R. Yakovlev, G.V. Astakhov, W. Ossau, S.A. Crooker, K. Uchida, N. Miura, A. Waag, N.A. Gippius, A.Y. Sivachenko, and A.B. Dzyubenko, Phys. Status Solidi A **227**, 353 (2001).
[13] D.R. Yakovlev, H.A. Nickel, B.D. McCombe, A. Keller, G.V. Astakhov, V.P. Kochereshko, W. Ossau, J. Nürnberger, F. Faschinger, and G. Landwehr, J. Cryst. Growth **214-215**, 823 (2000).
[14] D.R. Yakovlev, J. Puls, G.V. Mikhailov, G.V. Astakhov, V.P. Kochereshko, W. Ossau, J. Nürnberger, F. Faschinger, F. Henneberger, and G. Landwehr, Phys. Status Solidi A **178**, 501 (2000).
[15] H.P. Wagner, H.P. Tranitz, and R. Schuster, Phys. Rev. B **60**, 15 542 (1999).
[16] G.V. Astakhov, V.P. Kochereshko, D.R. Yakovlev, W. Ossau, J. Nürnberger, F. Faschinger, and G. Landwehr, Phys. Rev. B **62**, 10 345 (2000).
[17] C. Riva, F.M. Peeters, and K. Varga, Phys. Rev. B **61**, 13 873 (2000).
[18] H.J. Lozykowski and V.K. Shastri, J. Appl. Phys. **69**, 3235 (1991).
[19] H. Asai and K. Oe, J. Appl. Phys. **54**, 2052 (1983).
[20] B. König, U. Zehnder, D.R. Yakovlev, W. Ossau, T. Gerhard, M. Keim, A. Waag, and G. Landwehr, Phys. Rev. B **60**, 2653 (1999).
[21] T. Miyajima, F.P. Logue, J.F. Donegan, J. Hegarty, H. Okuyama, A. Ishibashi, and Y. Mori, Appl. Phys. Lett. **66**, 180 (1995).
[22] A. Ishibashi, J. Cryst. Growth **159**, 555 (1996).
[23] K. Shahzad, J. Petruzzello, J.M. Gaines, and C. Ponzoni, Appl. Phys. Lett. **67**, 659 (1995).
[24] Landolt-Börnstein, *II-IV and I-VI Compounds; Semimagnetic Compounds*, edited by U. Rössler, Vol. III/41B of *New Series* (Springer, Berlin, Heidelberg, 1999).
[25] T. Ohyama, K. Sakakibara, E. Otsuka, M. Isshiki, and K. Igaki, Phys. Rev. B **37**, 6153 (1988).
[26] H.W. Hölscher, A. Nöthe, and C. Uihlein, Phys. Rev. B **31**, 2379 (1985).
[27] H. Okuyama, Y. Kishita, T. Miyajima, A. Ishibashi, and K. Akimoto, Appl. Phys. Lett. **64**, 904 (1994).
[28] H. Okuyama, Y. Kishita, and A. Ishibashi, Phys. Rev. B **57**, 2257 (1998).
[29] M.T. Litz, M. Korn, H. Ress, U. Lunz, W. Ossau, A. Waag, G. Landwer, K. Watanabe, T. Walter, and B. Neubauer, J. Cryst. Growth **159**, 54 (1996).
[30] K. Wilmers, T. Wethkamp, N. Esser, C. Cobet, W. Richter, M. Cardona, V. Wagner, H. Lugauer, F. Fisher, and T. Gerhard, Phys. Rev. B **59**, 10 071 (1999).
[31] L. Vegard, Z. Phys. **5**, 17 (1921).
[32] S.A. Crooker, D.G. Rickel, S.K. Lyo, N. Samarth, and D.D. Awschalom, Phys. Rev. B **60**, R2173 (1999).
[33] N.A. Gippius, A.L. Yablonskii, A.B. Dzyubenko, S.G. Tikhodeev, L.V. Kulik, V.D. Kilakovskii, and A. Forchel, J. Appl. Phys. **83**, 5410 (1998).
[34] A.A. Sirenko, T. Ruf, M. Cardona, D.R. Yakovlev, W. Ossau, A. Waag, and G. Landwehr, Phys. Rev. B **56**, 2114 (1997).
[35] A.A. Kiselev, E.L. Ivchenko, A.A. Sirenko, T. Ruf, M. Cardona, D.R. Yakovlev, W. Ossau, A. Waag, and G. Landwehr, J. Cryst. Growth **184-185**, 831 (1998).
[36] D. Wolverson, J.J. Davies, C.L. Orange, K. Ogata, S. Fujita, K. Nakano, H. Okuyama, S. Itoh, B. Jobst, and D. Hommel, Phys. Rev. B **60**, 13 555 (1999).
[37] J.J. Davies, D. Wolverson, I.J. Griffin, O.Z. Karimov, C.L. Orange, D. Hommel, and M. Behringer, Phys. Rev. B **62**, 10 329 (2000).
[38] A. Naumov, D. Mi, M. Sturge, W. Ge, L.S. Dang, H. Mariette, and N. Magnea, J. Appl. Phys. **78**, 1196 (1995).
[39] A.J. Shields, J.L. Osborne, M.Y. Simmons, M. Pepper, and D.R. Ritchie, Phys. Rev. B **52**, R5523 (1995).
[40] P. Kossacki, J. Cibert, D. Ferrand, Y.M. d'Aubigne, A. Arnoult, A. Wasiela, S. Tatarenko, and J.A. Gaj, Phys. Rev. B **60**, 16 018 (1999).
[41] G.V. Astakhov, V. P. Kochereshko, D.R. Yakovlev, W. Ossau, J. Nürnberger, F. Faschinger, G. Landwehr, T. Wojtowicz, G. Karczewski, and J. Kossut, Phys. Rev. B **65**, 115310 (2000).
[42] In the case of ZnSe-based QW's scattering of the carriers generated by the above-barrier photoexcitation into the GaAs substrate can also contribute to the carrier redistribution during illumination. This effect might play a role for the structures of type's B and C, where the overall thickness of the ZnSe-based structure is relatively small (about 200 nm). However, we believe that this effect is of minor importance for the type A and D structures with thick ZnSe-based layers (total thickness of 750 nm), which are larger than the characteristic absorption length of the illumination photons of about 100 nm.
[43] A. Esser, E. Runger, R. Zimmermann, and W. Langbein, Phys. Rev. B **62**, 8232 (2000).
[44] V. Huard, R.T. Cox, K. Saminadayar, A. Arnoult, and S. Tatarenko, Phys. Rev. Lett. **84**, 187 (2000).
[45] R.A. Suris, V.P. Kochereshko, G.V. Astakhov, D.R. Yakovlev, W. Ossau, J. Nürnberger, F. Faschinger, G. Landwehr, T. Wojtowicz, and G. Karczewski, Phys. Status Solidi A **227**, 343 (2001).
[46] B. Stebe and A. Ainane, Superlattices Microstruct. **5**, 545 (1989).
[47] R.A. Sergeev and R.A. Suris, Fizika Tverdogo Tela **43**, 714 (2001) [Phys. Solid State **43**, 746 (2001)].
[48] B. Stebe, G. Munschy, L. Stauffer, F. Dujardin, and J. Murat, Phys. Rev. B **56**, 12 454 (1997).
[49] I. N. Yassievich, V. M. Chistyakov, and V.P. Kochereshko, in *Proceedings of the 24th International Conference on the Physics of Semiconductors, Jerusalem, Israel 1998*, Ref. 10.
[50] A. Esser (private communication).
[51] G. Finkelstein and I. Bar-Joseph, Nuovo Cimento D **17**, 1239 (1995).
[52] T. Taliercio, P. Lefebvre, V. Calvo, D. Scalbert, N. Magnea, H. Mathieu, and J. Allegre, Phys. Rev. B **58**, 15 408 (1998).
[53] T. Vanhoucke, M. Hayne, M. Henini, and V.V. Moshchalkov, Phys. Rev. B **63**, 125331 (2001).
[54] G. Yusa, H. Shtrikman, and I. Bar-Joseph, Phys. Rev. Lett. **87**, 216402 (2001).
[55] D.M. Whittaker and A.J. Shields, Phys. Rev. B **56**, 15 185 (1997).